Nuclear Instruments and Methods in Physics Research A296 (1990) 791–796
North-Holland

HIGH-AVERAGE-POWER CW FELs FOR APPLICATION TO PLASMA HEATING: DESIGNS AND EXPERIMENTS

J.H. BOOSKE *, V.L. GRANATSTEIN, D.J. RADACK, T.M. ANTONSEN, Jr., S.W. BIDWELL, Y. CARMEL, W.W. DESTLER, P.E. LATHAM, B. LEVUSH, I.D. MAYERGOYZ and Z.X. ZHANG

Laboratory for Plasma Research, University of Maryland, College Park, MD 20742, USA

H.P. FREUND

Science Applications International Corporation, McLean, VA 22102, USA

A short-period-wiggler (period ~1 cm), sheet-beam FEL has been proposed as a low-cost source of high-average-power (1 MW) millimeter-wave radiation for plasma heating and space-based radar applications. Recent calculations and experiments have confirmed the feasibility of this concept in such critical areas as rf wall heating, intercepted beam ("body") current, and high-voltage (0.5–1 MV) sheet-beam generation and propagation. Results of preliminary low-gain sheet-beam FEL oscillator experiments using a field-emission diode and pulse line accelerator have verified that lasing occurs at the predicted FEL frequency. Measured start oscillation currents also appear consistent with theoretical estimates. Finally, we consider the possibilities of using a short-period, superconducting planar wiggler for improved beam confinement, as well as access to the high-gain, strong-pump Compton regime with its potential for highly efficient FEL operation.

1. Introduction

The use of a small-period planar-wiggler ($l_w \approx 1$ cm) free-electron-laser (FEL) oscillator together with a sheet electron beam has been proposed as a low-cost source of power for electron cyclotron resonance heating (ECRH) in magnetic fusion plasmas [1]. Other potential applications include space-based radar systems [1]. In previous work, we have established the feasibility of stable sheet-beam confinement using wiggler focusing [2] and developed a "universal", self-consistent design method for low-gain, Compton-regime, untapered FEL oscillators [3,4]. The highly flexible design procedure has taken into account sheet-beam space-charge effects on gain [5], axial-mode competition and stability [6], transverse-mode control techniques [5], and dynamic evolution from oscillator noise to saturated equilibrium, including finite beam voltage rise-time effects [7]. Examples of several 300 GHz, 1 MW cw oscillator designs derived rapidly with the universal procedure are presented in table 1. The three designs span beam voltages from 650 to 1000 kV. We will describe and refer to the various parameters in this table periodically throughout the paper.

Much of our recent work has concentrated on applied studies to assess technological risk and feasibility issues in the proposed cw FEL system. A comprehensive review of our results will be published in ref. [8]. Here we will concentrate on the specific issues of thermal management, body currents, and high-voltage sheet-beam thermionic gun design. Furthermore, we will discuss the results of preliminary short-pulse low-gain sheet-beam FEL oscillator experiments (using a short-period wiggler), as well as the predicted possibilities for using superconducting (SC) short-period planar wigglers to enhance beam confinement and to access a high-gain, strong-pump Compton regime of operation.

2. Thermal management and body currents

In previous studies [4], we established that the short-period wiggler FEL configuration was conservatively compatible with steady-state thermal cooling of cavity walls up to 1.5 kW/cm^2. By selecting oscillators based on slightly higher beam voltages – and thus larger wiggler periods and cavity gaps – we have identified FEL designs with extremely small rf ohmic wall losses. Referring specifically to table 1, we note that at higher beam voltages, rf ohmic heat dissipation may reach levels below 10 W/cm^2. Measurements on our electromagnetic small-period wigglers (cf. ref. [9]) indicate that bulk ohmic magnet heating under dc operation will be readily manageable and should not contribute to additional temperature elevation of the cavity wall. Fur-

* Permanent address: E.C.E. Department, University of Wisconsin, Madison, WI 53706, USA.

Table 1
1 MW, 300 GHz untapered FEL oscillator designs

V_{beam} [kV]	650	850	1000
I_{beam} [A]	48	40	34
b_{beam} [cm] [a]	0.20	0.24	0.26
a_{beam} [cm]	4.0	4.0	4.0
θ_{beam} [deg]	±2.0	±2.0	±2.0
b_{rf} [cm]	0.375	0.575	0.70
a_{rf} [cm]	5.5	6.0	6.0
T_{eff}	0.13	0.11	0.12
L [cm]	19.6	25	30
l_w [cm]	0.85	1.25	1.50
N_w [# periods]	23	20	20
B_w [kG]	2.0	2.0	2.0
λ_β [cm]	15.5	18.7	21.1
f [GHz]	285	288	300
η_e	3.0%	3.1%	3.0%
$\delta\gamma_z/(\gamma_z-1)$ (total)	±0.8%	±0.8%	±1.0%
beam/wall clearance [mm]	0.88	1.7	2.2
$\theta_{intercept}$ [deg]	±3.5	±5.5	±6.0
$\hat{P}^{rf}_{wall}$ [W/cm^2] [b,c]	72	24	<10
P_{cav} [MW]	6.9	9.3	<8.9
P_{out} [MW]	0.90	1.00	1.02
η_T (92% beam energy recovery)	28%	28%	28%
ϕ_{LV} [kV]	71.5	93.5	110

[a] Injected beam thickness is 1 mm in all cases.
[b] Used σ-values reduced ×2 from textbook values.
[c] Maximum estimated cooling capability ~1.5 kW/cm^2.

thermore, recent advances in small-period wiggler technology [10] indicate that either permanent- or superconducting-magnet technology may be appropriate for the compact planar geometry of our FEL designs. In such cases, the issue of thermal management of magnet-generated heat is moot.

The remaining agent for thermal stress of the cavity waveguide walls, then, is body current. Having already established that relativistic sheet beams propagate stably under wiggler focusing [1,2], we turned to the question of how much fractional body current would intercept the waveguide walls for a given set of design parameters. The various causes of beam interception include ballistic motion, space-charge expansion, orbit perturbation by the rf radiation fields, and wiggler field errors. We will discuss the first three body current mechanisms in this paper. The effect of wiggler field errors will be addressed in a later publication.

A "Brillouin" equilibrium condition for wiggler confinement of a laminar sheet beam against space-charge expansion can be derived as [2]

$$\omega_p^2 = \frac{\gamma_z^2}{2\gamma}\Omega_w^2, \tag{1}$$

where $\omega_p^2 = 4\pi ne^2/m$ and $\Omega_w = eB_w/mc$. For quantitative purposes, eq. (1) can be written as

$$J_b\left[\mathrm{A/cm^2}\right] = 232\gamma\beta B_w^2, \tag{2}$$

where B_w, the wiggler field amplitude, is in kG and J_b is the "Brillouin" equilibrium current density. In all cases, our sheet-beam FEL designs are specified such that the injected beam current density is less than one order of magnitude smaller than the Brillouin current density. Thus, the wiggler focusing forces greatly dominate the space-charge forces and space charge is not a determining factor in fractional body currents.

Ballistic motion of single-electron orbits can be conservatively estimated to follow the periodic betatron-orbit solution [8]:

$$y(z) = \mathscr{y}_\beta \sin\left(\frac{2\pi z}{\lambda_\beta} + \Psi_\beta\right), \tag{3}$$

where

$$\mathscr{y}_\beta = \sqrt{y_0^2 + \left(\frac{\lambda_\beta\theta_{y0}}{2\pi}\right)^2},$$

$$\Psi_\beta = \tan^{-1}\left(\frac{2\pi y_0}{\lambda_\beta\theta_{y0}}\right),$$

$$\lambda_\beta = \frac{m\gamma\beta c\sqrt{2}}{eB_w},$$

and y_0 and θ_{y0} are the injected electron's transverse position and the divergence angle, respectively. Accordingly, electron interception of the waveguide wall will be avoided if the betatron amplitude is kept smaller than one-half of the waveguide gap dimension, i.e.,

$$\mathscr{y}_\beta < b_{rf}/2. \tag{4}$$

For the beam parameters described in the section on gun design, the betatron amplitude confinement condition is predicted to be sufficiently satisfied such that the ballistic component of body current is estimated to be μA or less.

Finally, we have looked at the issue of body currents induced by rf fields and entrance wiggler tapers by performing three-dimensional simulations of electron trajectories in the presence of combined wiggler and electromagnetic wave fields. Initial conditions for the injected electrons included finite beam thickness effects, as well as a distribution of pitch angles. The pitch angle distribution was a consequence of assuming an energy distribution of the form

$$f(\gamma_z) \approx \exp\left[-(\gamma_0 - \gamma_z)^2/(\Delta\gamma_z)^2\right], \tag{5}$$

where the total energy is constant: $\gamma_y + \gamma_z = \gamma_0$. Sample results of simulations for the 1 MV FEL design of table 1 (performed with sufficient particles to yield statistically accurate results) are plotted in fig. 1. As evident, the fractional interception can be plotted as contours in either $\Delta\gamma_z/\gamma_0$ versus y phase space, or a θ_{y0} versus y trace space. The shaded region marked "no particle loss" is qualitatively and quantitatively consistent with the analytic prediction obtained from eqs. (3) and (4).

Thus, the first, most important prediction is that, consistent with intuition, a sufficiently low-emittance beam will suffer negligible body current. In addition, the simulations have found that for an injected beam quality which satisfies the unperturbed (i.e., no rf field) confinement conditions, there is no significant increase in body current due to the addition of the rf fields. This is a consequence of using high-voltage, low-current-density – and thus very "stiff" – electron beams. The other observation from the simulations was that too long an entrance wiggler taper resulted in severe limits on beam emittance to avoid body current. For the beam and wiggler parameters of table 1, however, a short one- or two-half-period taper will be adequate for beam entrance matching without increasing body current.

To verify the predictions on body currents we have performed sheet-beam transport experiments based on slight modifications to the early configuration of ref. [2]. Since the details of these experiments are described more fully in ref. [11], we will summarize the results below. The modifications to the configuration of ref. [2] included electrically isolating the waveguide body in order to measure small body currents, as well as replacing the series of small holes in the masking with a 1 mm thick rectangular slit. Thus, for these experiments the injected beam was a true sheet beam. By deliberate, careful experimental techniques, we obtained a minimum fractional body current resolution capability of $I_{body}/I_{beam} < 0.5\%$. The body currents were measured for 500 kV beams under two conditions: (1) a high-current-density ($J \approx 0.5$–1.5 kA/cm^2), large-emittance ($\theta_{y0} \lesssim \pm 5°$) beam and (2) a low-current-density ($J \approx 7.5$–15 A/cm^2), low-emittance ($\theta_{y0} \lesssim \pm 1°$) beam. The fractional body current data is plotted in fig. 2. The "single-anode beam" data corresponds to the high-current-density, large-emittance conditions, while the "double-anode beam" data corresponds to the low-current-density, low-emittance conditions. The experimental results agreed well with the theoretical predictions in the following ways. First the "single-anode beam" had a current density of the order of the Brillouin current density of eq. (2). Furthermore, this same beam had a significant fraction of electron current which exceeded the ballistic confinement conditions of eqs. (3) and (4). Consequently, as expected, roughly 20% body current was measured for this beam at wiggler fields as high as 2 kG. The "double-anode beam", on the other hand, had a current density one order of magnitude less than the Brillouin value, as well as an injected electron emittance which satisfied the ballistic confinement condition of eqs. (3) and (4) by a wide margin. Therefore, in agreement with predictions, the body current for this beam was essentially zero within the resolution of the measurement.

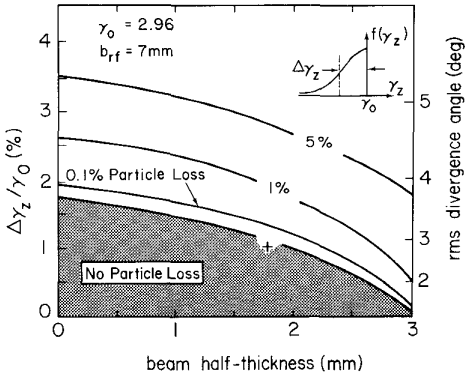

Fig. 1. Fractional body current contours in both energy-position phase space and pitch (divergence) angle versus position trace space. Data resulted from 3D trajectory simulations for the 1 MV FEL design in table 1. Point marked with a cross (+) is a conservation characterization of a predicted sheet-beam gun design.

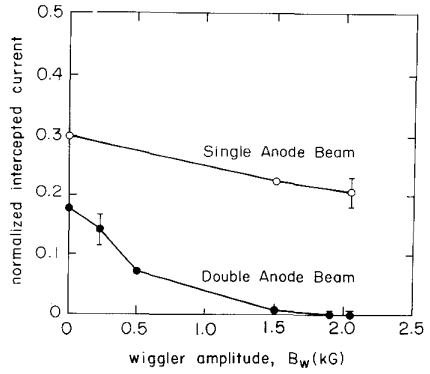

Fig. 2. Fractional body current for two ~ 500 kV sheet beams as a function of wiggler-focusing field amplitude. The "double-anode beam" had much lower emittance and current density than the "single-anode beam".

3. High-voltage sheet-beam thermionic gun design

From the previous discussion, one can determine that the proposed FEL will require a cw thermionic "Pierce" gun with an injected-beam thickness $b_{beam} \approx 1$ mm, beam voltage $V_{beam} \approx 0.5$–1.0 MV, linear current density $i_{beam} \approx 7.5$–15.0 A/cm (area current density $J_{beam} \approx 75$–150 A/cm^2), and a maximum pitch angle at injection of $\theta_{beam} \lesssim \pm 2°$. Present state-of-the-art [12] sets the maximum electric field for cw operation at ~ 100 kV/cm. To realize the maximum FEL intrinsic (electronic) efficiency requires the beam energy spread in the interaction region to be $\Delta\gamma_z/(\gamma_z - 1) \lesssim \pm 2\%$ [3].

Our preliminary gun design studies have established that a multianode electrostatically focused sheet-beam gun should be suitable. A sample simulation of the gun

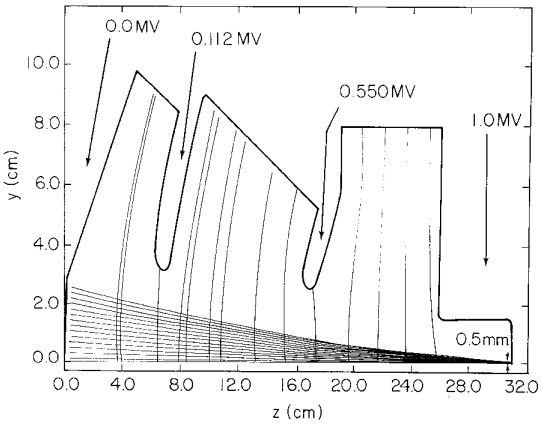

Fig. 3. Sample simulation of a 0.7–1.0 MV sheet-beam thermionic gun design using multianode electrostatic focusing. The solution shown was a nonthermal solution based on 14 rays. Little change was found when using more rays (up to 98) or by varying the final anode voltage over a ~ 200–300 kV range.

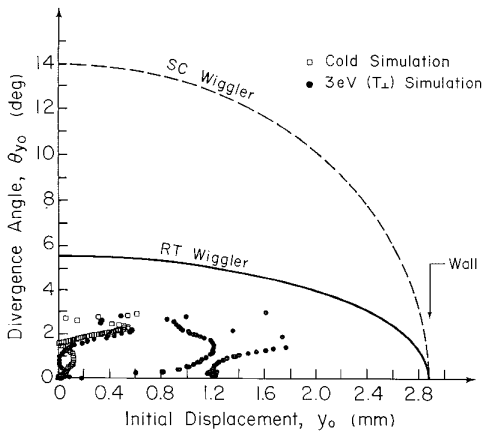

Fig. 4. Trace space for both nonthermal (open squares) and (3 eV) thermal (dark circles) beam solutions of the gun in fig. 3. The solid boundary represents the analytic ballistic confinement limit for the 850 kV FEL design using a 2 kG (i.e., room-temperature) wiggler. The dashed boundary is the same confinement limit using a 6 kG (superconducting) wiggler.

for 1 MV operation is shown in fig. 3. The beam characteristics at the gun exit are tabulated in table 2 alongside the desired specifications mentioned earlier. It is evident from the table that almost all of the desired specifications have been equaled or exceeded by this first design effort, with the exception of the current density. It is expected that the additional desired 50% increase in the current density will be readily achieved in future systematic gun simulation studies.

The simulations of the gun in fig. 3 were performed both for a nonthermal solution (using 98 rays) as well as a 3 eV thermal-beam solution (using a 3-ray-split technique described in ref. [13]). Typical cathode temperatures will generally be of order 0.1 eV, i.e., much less than 3 eV. The basis of considering a 3 eV transverse beam temperature is that this represents a very conservative estimate of finite beam temperature resulting from cathode surface roughness [8,14]. The loci of the rays at the gun exit are plotted in the trace space of fig. 4. Also plotted in fig. 4 is the analytic ballistic confinement boundary described in eqs. (3) and (4) (at this point we specifically refer to the solid boundary marked "RT wiggler" corresponding to a 2 kG room-temperature wiggler field). Note that even for the 3 eV simulation, all rays fall well within the solid confinement boundary. The rms beam half-thickness and divergence angle for the 3 eV simulation are approximately 0.7 mm and 2°, respectively (this is a little misleading, since the beam distributions tend to be more flat-top than Gaussian – thus the characterization using a Gaussian is a conservative one). Conservatively overestimating these two parameters as 1.8 mm and 3°, respectively, (corresponding to the outermost ray in fig. 4) yields a beam that still falls within the zero-body-current regime. This is indicated by the point marked with a cross (+) in fig. 1. Recall that fig. 1 was generated with simulations that included the body currents resulting from rf-induced orbit perturbations, as well as beam-matching entrance tapers on the wiggler.

Table 2
Sheet-beam gun characteristics

Quantity	Desired spec.	1st-cut design value
Thickness [mm]	1.0	1.0
Beam voltage [MV]	0.5–1.0	0.7–1.0
Voltage tuning [kV]	≥ 100	300
Linear current density [A/cm]	7.5–15	5.0
Divergence angle [deg]	≤ ±2	≤ ±3
Maximum electric field [kV/cm]	≤ 100	≤ 70
Beam energy spread [%]	≈ 0	< 0.05
Axial energy spread in FEL [%]	< ±2	±(1.2–1.9)
Cathode emission current density [A/cm^2]	< 10	~ 1

4. Short-pulse, sheet-beam, SPW FEL oscillator experiments

By adding a copper "end-cap" to the waveguide used in the beam transport experiments of refs. [2] and [11], we converted the configuration to a low-gain, short-pulse

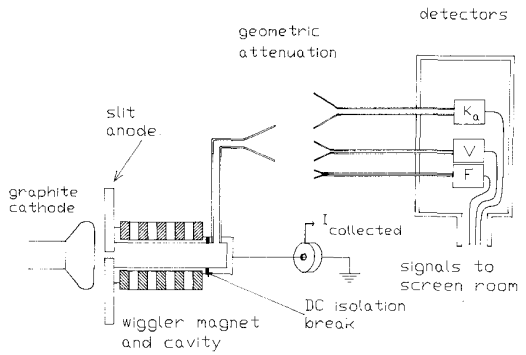

Fig. 5. SPW sheet-beam FEL oscillator configuration used in preliminary experiments with a pulse-line accelerator injector.

oscillator. The oscillator configuration schematic is shown in fig. 5. The same wiggler/cavity arrangement has been used in preliminary experiments on both 30 and 100 ns pulse-line accelerator injectors using field-emission diodes. Neither beam pulse duration is sufficient for oscillator saturation. Furthermore, neither pulse has a sufficiently flat voltage pulse for optimum interaction efficiency. Nevertheless, initial lasing experiments on these systems provide us with useful information on lasing frequencies and start oscillation currents which can be compared with theoretical predictions.

The first experiments were performed on the same 30 ns pulse-like accelerator as used in the beam-transport experiments of refs. [2] and [11]. A definite correlation between detected radiation and wiggler field intensity was established as shown in fig. 6. These particular experiments were performed with a beam energy of approximately 300 kV and a beam current of approximately 100–150 A. Using waveguide cutoff filter techniques, it was established that the majority of the detected signal was in the 40–70 GHz frequency band. This is consistent with a grazing FEL interaction in a TE_{01} transverse waveguide mode for the particular experimental parameters. The same FEL oscillator configuration has been moved to a 100 ns pulse-line accelerator system which has the capability of much flatter beam voltage during the pulse duration, provided a proper match is achieved between the diode and the injector's pulse transmission line. While this work is just getting under way, the preliminary data displayed in fig. 7 indicates that start oscillation currents are of order 50 A. For the experimental parameters chosen, this would be in approximate agreement with the formula [3]

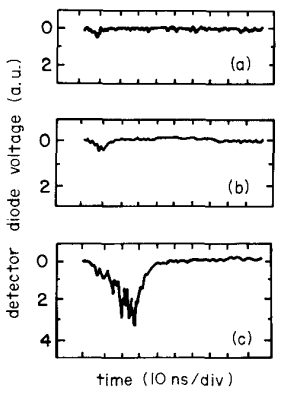

Fig. 6. Correlation between FEL radiation detector signal and wiggler field strength: (a) $B_w = 0$ kG, (b) $B_w = 0.8$ kG, (c) $B_w = 1.5$ kG.

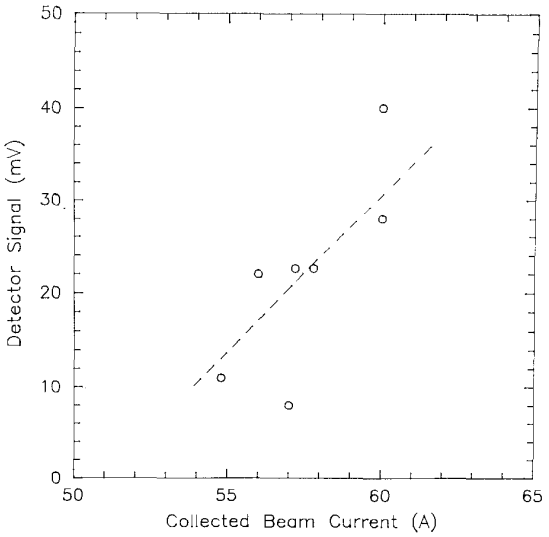

Fig. 7. Correlation between FEL radiation detector signal and collected beam current, indicating a start oscillation current of approximately 50 A.

$$I_{start} \approx 15\left(\frac{k_z\omega}{4\pi}\right) a_{rf} b_{rf} \left(\frac{mc^2}{e}\right)\left(\frac{c}{\omega}\right)^3 \frac{\left(\gamma_0^2 - 1\right)^{5/2} T_{eff}}{L^3 a_w^2 \left(1 + \frac{1}{2}a_w^2\right)}, \quad (6)$$

for an effective transmission coefficient of $T_{eff} \approx 0.01$. Measurements of the cavity transmission losses are presently in progress. Nevertheless, the small value of T_{eff} mentioned above would be consistent with the small output couping hole and masking anode slit used in the experiment.

5. Superconducting SPW sheet-beam FEL

Recent advances in superconducting (SC) wiggler research indicate that it may be practical to construct short-period ($l_w \approx 1$ cm) planar wigglers using NbTi SC windings [10,14]. This would open up exciting new

possibilities for the SPW sheet-beam FEL. As an example, we consider the following parameters: $V_{beam} \approx 1$ MV, $B_w \approx 6$ kG, $l_w \approx 1$ cm, $a_{beam} \approx 4$ cm, $b_{beam} \approx 0.2$ cm, $L \approx 0.5$–1.0 m and $I_{beam} \approx 4$ A. Note that the wiggler parameters are very similar to those specified for a SC planar wiggler being constructed at Brookhaven National Laboratory [14]. The first advantage of using the SC wiggler is the considerably improved beam confinement indicated by the dashed ballistic confinement boundary marked "SC wiggler" in the trace space of fig. 4. The second possibility is that a SC magnet may make it possible for the SPW sheet-beam FEL to operate in the strong-pump regime (high-gain, noncollective) where based on previous experience [15], tapering may be used to yield efficiencies of 30–40%.

First, for the example parameters cited above, the accessible FEL operating frequency is ≥ 300 GHz. Based on the formulas in ref. [16], the strong-pump operation will occur when

$$-\mathrm{Im}(k)L \gg 1 \tag{7}$$

and

$$a_w/\gamma_0 \gg \beta_{crit}, \tag{8}$$

where

$$\beta_{crit} = 4\left[\tilde{\omega}_p/ck_w\gamma_0^2\right]^{1/2}, \tag{9}$$

$$\tilde{\omega}_p^2 = 4\pi ne^2/m\gamma_0^3, \tag{10}$$

and

$$-\mathrm{Im}(k) = 0.687\left(\tilde{\omega}_p a_w/ck_w\right)^{2/3}k_w. \tag{11}$$

For the parameters specified we calculate

$a_w/\gamma_0 \approx 0.19$,

$\beta_{crit} \approx 0.068$,

and

$-\mathrm{Im}(k)L \approx 2.25$–$4.52$.

Thus, both eqs. (7) and (8) should be satisfied. For tapered efficiencies of 30–40%, the output power would be approximately 1.2–1.6 MW per device. If depressed collectors with spent beam collection efficiency of 60–70% were possible, the resulting total system efficiency would be approximately 50%. Finally, based on the linear gain estimates, using the sheet-beam SPW FEL in an amplifier configuration would correspond to power amplification of 30–40 dB. Thus, an input gyrotron oscillator of 100–100 W cw would be sufficient to achieve the desired 1 MW output power. We are presently studying the question of the actual length of such an amplifier design, including the tapering. Note that the sheet-beam SPW FEL amplifier should have the same low rf wall losses as predicted for the oscillator designs in table 1. Furthermore, although the amplifier interaction region would be significantly longer than for the low-gain oscillator designs, the body current should still be manageable, due to the improved beam confinement and the lower total beam current associated with the SC wiggler FEL amplifier.

References

[1] V.L. Granatstein, T.M. Antonsen, jr., J.H. Booske, W.W. Destler, P.E. Latham, B. Levush, I.D. Mayergoyz, D.J. Radack, Z. Segalov and A. Serbeto, Nucl. Instr. and Meth. A272 (1988) 110.

[2] J.H. Booske, W.W. Destler, Z. Segalov, D.J. Radack, E.T. Rosenbury, J. Rodgers, T.M. Antonsen, Jr., V.L. Granatstein and I.D. Mayergoyz, J. Appl. Phys. 64 (1988) 6.

[3] J.H. Booske, A. Serbeto, T.M. Antonsen, Jr. and B. Levush, J. Appl. Phys. 65 (1989) 1453.

[4] J.H. Booske, V.L. Granatstein, T.M. Antonsen, Jr., W.W. Destler, J. Finn, P.E. Latham, B. Levush, I.D. Mayergoyz, D. Radack, J. Rodgers, M.E. Read and A. Linz, Nucl. Instr. and Meth. A285 (1989) 92.

[5] T.M. Antonsen, Jr. and P.E. Latham, Phys. Fluids 31 (1988) 3379.

[6] T.M. Antonsen, Jr. and B. Levush, Phys. Fluids B1 (1989) 1907.

[7] T.M. Antonsen, Jr. and B. Levush, Phys. Rev. Lett. 62 (1989) 1488.

[8] J.H. Booske, D.J. Radack, T.M. Antonsen, Jr., S. Bidwell, Y. Carmel, W.W. Destler, H.P. Freund, V.L. Granatstein, P.E. Latham, B. Levush, I.D. Mayergoyz, A. Serbeto and Z.X. Zhang, IEEE Trans. Plasma Sci. (3rd Special Issue on High Power Microwave Generation (1989)) PS-18 (1990) 399.

[9] W.W. Destler, V.L. Granatstein, I.d. Mayergoyz and Z. Segalov, J. Appl. Phys. 60 (1986) 521.

[10] R.L. Sheffield, J.H. Booske, R.W. Warren, K. Halbach, B. Danly, R. Jackson, P. Walstrom, J. Slater and A. Toor, presented at this Conference (11th Int. Free Electron Laser Conf., Naples, FL, USA, 1989).

[11] D.J. Radack, J.H. Booske, Y. Carmel and W.W. Destler, Appl. Phys. Lett. 55 (1989) 2069.

[12] G. Miram, Varian, private communications (1988).

[13] R. True, IEEE Trans. Electron Devices ED-34 (1987) 473.

[14] K. Batchelor, I. Ben-Zvi, R. Fernow, J. Gallardo, H. Kirk, C. Pellegrini and A. Van Steenbergen, these Proceedings (11th Int. Free Electron Laser Conf., Naples, FL, USA, 1989) Nucl. Instr. and Meth. A296 (1990) 239.

[15] T.J. Orzechowski, B.R. Anderson, J.C. Clark, W.M. Fawley, A.C. Paul, D. Prosnitz, E.T. Scharlemann, S.M. Yarema, D.B. Hopkins, A.M. Sessler and J.S. Wurtele, Phys. Rev. Lett. 57 (1986) 2172.

[16] P. Sprangle, R.A. Smith and V.L. Granatstein, in: Infrared and Millimeter Waves, vol. 1, ed. K. Button (Academic Press, 1979) pp. 279–327.